Marine Geology 451 (2022) 106885

Contents lists available at ScienceDirect

Marine Geology

journal homepage: www.elsevier.com/locate/margo

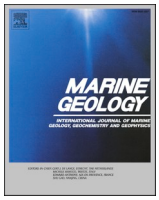

Research Article

Evolution of a single incised valley related to inherited geology, sea level rise and climate changes during the Holocene (Tirso river, Sardinia, western Mediterranean Sea)

Giovanni De Falco [a,*], Alfredo Carannante [b], Carla Del Vais [c], Luca Gasperini [d], Vincenzo Pascucci [e], Ignazio Sanna [f], Simone Simeone [a], Alessandro Conforti [a]

[a] CNR-IAS, Istituto per lo studio degli Impatti Antropici e Sostenibilità in ambiente marino, Sede Secondaria Oristano, Località Sa Mardini, 09170 Torregrande, Oristano, Italy
[b] International Research Institute for Archaeology and Ethnology, Napoli, Italy
[c] Università degli Studi di Cagliari, Dipartimento di Lettere, Lingue e Beni Culturali, Cittadella dei Musei, Piazza Arsenale 1, 09124 Cagliari, Italy
[d] CNR-ISMAR, Istituto di Scienze Marine, Sede Secondaria Bologna, Via Gobetti 101, 40129 Bologna, Italy
[e] Università degli Studi di Sassari, DADU-Dipartimento di Architettura, Design e Urbanistica Palazzo del PouSalit, Piazza Duomo, 6 I-07041 Alghero (SS), Italy
[f] Soprintendenza ABAP per la città metropolitana di Cagliari e le province di Oristano e Sud Sardegna, Piazza Indipendenza 7, 09124 Cagliari, Italy

ARTICLE INFO

Keywords:
Incised valley
Holocene
Geological control

ABSTRACT

We performed a morpho-stratigraphic study of the Tirso River incised valley (Sardinia Island, western Mediterranean Sea), an erosional feature crossing the Sinis fault, a major normal fault bordering the Campidano basin between the Gulf of Oristano and the western Sardinia shelf. High-resolution seismic reflection profiles and multibeam echosounder data, integrated by age-constrained stratigraphic logs derived from 9 sediment cores enabled us to reconstruct the valley evolution during the Holocene. We found that the Tirso valley is the result of a single event of incision and infill during the last eustatic cycle, strongly controlled by the presence of the Sinis fault. In fact, this structure represents a geological threshold that marks an abrupt change in substrate lithology and seabed slope, which controlled the valley morphology, narrow when downcutting early Pliocene formations along the steeper open shelf, and wider inside the Gulf, in the Pleistocene alluvial deposits of the flatter Gulf of Oristano. The sedimentary record starts with alluvial sediments filling the valley along the shelf during the initial phase of sea level rise, i.e., over 10 ka. During the last ~9.0 ka, a bay head delta developed, with the formation of barriers at the gulf entrance. In the mid-late Holocene, the progressive sea-level rise led to rapid drowning of the barrier system, recorded by marine and estuarine sediments filling the valley. Analysis of ecological associations in the cores, collected along a valley-normal transect, allowed for a detailed reconstruction of the paleo-environmental conditions during the latest phase of the incised valley filling controlled by global climatic variations in the Mediterranean region between ~9.0 and ~ 4.5 ka. Together with eustasy, our work reveals that the evolution and sedimentary infill of the Tirso incised valley was strongly controlled by inherited geological constraints, which influenced the morphology of the valley and the stratigraphic pattern.

1. Introduction

Incised valley systems are elongated fluvially-eroded topographic lows (Zaitlin et al., 1994), which are common along the modern shelves of the word (Allen and Posamentier, 1993; Flood et al., 2009; Green, 2009; Labaune et al., 2010; Simms et al., 2010; Maselli and Trincardi, 2013; Traini et al., 2013; Gomes et al., 2016; Qiu et al., 2019). These incised valleys formed as consequence of shelf exposure related to relative sea-level falls, which led to the basinward migration of the fluvial systems (Schumm, 1993; Martin et al., 2011).

Many sequence and seismic stratigraphic studies have been carried out on incised valley systems of the last few decades due to their importance as potential hydrocarbon reservoirs and paleo-climate archives (Blum et al., 2013; Wang et al., 2020). Moreover, the fills of late Quaternary incised valleys are among the few transgressive deposits preserved during shelf ravinement and give the possibility to investigate

* Corresponding author.
E-mail address: giovanni.defalco@cnr.it (G. De Falco).

https://doi.org/10.1016/j.margeo.2022.106885
Received 11 May 2022; Received in revised form 4 August 2022; Accepted 11 August 2022
Available online 17 August 2022

environmental changes occurred during late Pleistocene-Holocene times (Simms et al., 2010; Maselli and Trincardi, 2013).

Lowstand fluvial systems may be unincised or may form incised valleys. In either case, when the margins are characterized by sea-level fall, the fluvial sediments bypass the coastal plain and alluvial plain, either through incised valleys or through unincised channels superimposed on the old sea floor (Posamentier, 2001; Green et al., 2013; Blum et al., 2013). The formation of an incised valley can occur when relative sea-level falls below a pronounced gradient knickpoint that can be represented by the depositional shoreline break, the shelf break, or by a tectonic scarp (Posamentier, 2001; Maselli and Trincardi, 2013; Gomes et al., 2016). Furthermore, the incised valley fills are classified as either simple or compound fills depending on the absence or presence of polycyclic episodes of incisions and related sequence boundaries (Zaitlin et al., 1994; Burger et al., 2001).

A landward shift of the depositional environments across a basal sequence boundary of regional extent, considered here as the subaerial unconformity, characterise the common stratigraphic organization of incised valley systems. The stratigraphic stacking of seaward (or outer segment, sensu Zaitlin et al., 1994) deposits is characterized by lowstand to transgressive fluvial units overlain by transgressive estuarine and marine units, which can include barrier-islands and bay-head delta deposits (Anthony et al., 2002; Maselli et al., 2014). These may be covered by highstand marine units, typically of the shoreface. Lowstand to transgressive successions of fluvial and estuarine deposits generally fill the landward sector of the valleys (Zaitlin et al., 1994, and reference therein). Recent studies showed that highstand bay-head delta deposits may also cap the inner-mid sector of the valley (Green et al., 2015).

Many case studies in different geological settings showed that the morphology and fills of incised valley experience significant deviations from the classical models due to the interplay of several factors (Blum et al., 2013). Site-specific factors may include the geological inheritance (e.g. Gomes et al., 2016; Lobo et al., 2017; Dladla et al., 2019), the shelf gradient (Matthews and Rodriguez, 2011; Green et al., 2013), the size and geomorphology of drainage basin (Matthews and Rodriguez, 2011) and the sediment supply and oceanographic regime (Anthony et al., 2014; Cartelle et al., 2022). Global factors include global sea level control and climate variability in turn conditioning sediment fluxes. Global sea level variations on millennial to sub-millennial scales can influence the stratigraphic architecture of incised valley infill and Holocene coastal systems (Tanabe et al., 2003, 2015; Amorosi et al., 2017; Pascucci et al., 2018). Climate variations during the Late Pleistocene-Holocene could allow variations of sediment supply, depositional environments and stratigraphic patterns of incised valleys and associated coastal plains (Simms et al., 2010; Maselli et al., 2014; Sarti et al., 2015).

The literature on incised valleys mainly concerns high sediment supply systems, which are generally filled by lowstand to highstand succession. Examples of low sediment supply systems include Kosi Estuary and incised valleys along the southern KwaZulu-Natal continental shelf (Cooper et al., 2012; Pretorius et al., 2019). These studies reveal that incised valleys characterized by low sediment supply are underfilled and contain lowstand and highstand systems tracts but lack a transgressive systems tract (Cooper et al., 2012; Pretorius et al., 2019).

Only a limited number of studies focused on geological controls that determine the geometry of nearshore incised valleys and their fills (Wang et al., 2019; Engelbrecht et al., 2020; Ximenes Neto et al., 2022). Tectonic tilting or uplift can cause accelerated stream flow and consequent erosion and incision (Posamentier, 2001). Gomes et al. (2016) showed that the structural heritage and pre-valley lithology influenced the shaping, and in consequence, the stratigraphic organization of the valley fill, of the Assu incised valley, of the equatorial Brazilian shelf.

In this paper we analyse the morphology and sedimentary infill of the Tirso River Incised Valley (TIV), located along the western coast of Sardinia Island (Mediterranean Sea). The TIV crosses the main fault of a structural depression of regional extent and represents a case study of an incised valley, in which evolution and infilling were conditioned by a structural control. The aim of this study is to show how the tectonic setting can determine abrupt changes in the valley morphology and in the sedimentary filling of the incised valley systems.

2. Study site

2.1. Geological setting

The TIV is located in the northern sector of the Campidano plain, it crosses the Gulf of Oristano and runs along the western shelf of Sardinia (Fig. 1). The Campidano basin is a Pliocene-Quaternary, NW-SE-oriented structural depression (Casula et al., 2001). The Campidano basin is bounded to the west by the Sinis fault, a master fault dipping to the east, which crosses the Gulf of Oristano between the two headlands that delimit it: Cape San Marco to the north and Cape Frasca to the south (Fig. 1; Casula et al., 2001). The Sinis fault is a normal fault with a maximum throw of about 1000 m (Cocco et al., 2013; Casula et al., 2001) which was active between the Pliocene and Pleistocene and is related to the extensive tectonic activity that affected southwestern Sardinia as a consequence of the Pliocene-Quaternary opening of the southern Tyrrhenian back-arc basin (Casula et al., 2001).

To the west of the Gulf of Oristano, the inner continental shelf is set on volcanic and marine deposits of the Miocene to Lower Pliocene, covered by a veneer of Quaternary sediments (Conforti et al., 2016). To the East, in the Gulf of Oristano, Miocene to Early Pliocene marine deposits were downthrow by about 1000 m following the opening of the Campidano basin. The basin which was filled by *syn*-rift continental deposits is interspersed by Pliocene basaltic lava flows (Casula et al., 2001) and is considered stable since the Middle Pleistocene (post 700 ka) (Cherchi et al., 2008). However, a recent study provided evidence of ongoing tectonic activity since the Marine Isotopic Stage 7 (MIS7; ca. 220 ka) on the structural high that bounds the north-western side of the Campidano Basin revealing the presence of N-S striking normal faults system (Tharros fault, Fig. 1) offsetting late Pleistocene aeolianites (130 $\pm$ 12 ka; 82 $\pm$ 9 ka) (Cocco et al., 2019).

The geological setting of the coastal plain includes terraced coarse Pleistocene deposits in the inner sector, and Holocene littoral, alluvial and lagoonal deposits along the coastal sector and the alluvial plain (Fig. 2).

The morphology of the TIV is clearly detectable from the bathymetry of the Gulf of Oristano (Fig. 1), between the Torregrande beach, located at north of the river mouth, and the entrance of the Gulf of Oristano. The surface sediment distribution in the northern sector of the Gulf includes the presence of a lobe of sandy-muddy sediments at the head of the incised valley (De Falco et al., 2006, 2008), mixed bioclastic muddy sands associated with seagrass meadows to the North (De Falco et al., 2000) and coarse siliciclastic sediments to the West, toward the Gulf entrance (De Falco et al., 2008, 2010). Here, there is a well-preserved submerged barrier-lagoon system, comprising several beachrocks at depths of 18–37 m and a wide back-barrier basin filled by fine sediments (De Falco et al., 2015a), that developed during the early Holocene. Seaward, outside the Gulf, the incised valley loses its morphological imprint on the seafloor. In this sector the incised valley cuts the Pliocene marine deposits, and it is filled by coarse alluvial deposits (De Falco et al., 2015a).

2.2. Drainage system and oceanographic feature

The drainage system of the northern side of the Campidano plain includes three major rivers (Fig. 1). The Tirso River, 150 km long, has the widest basin with a catchment area of ca. 3340 km^2. The river crosses a hilly area up to ca. 20 km from the mouth where a knick-point characterizes the entrance of the river to the alluvial plain. The river has a torrent-like regime with maximum inflow during the wet season. Several dams are present in the catchment areas and the flood flow at the mouth is presently evaluated at 536 m^3 s^{-1} and 3870 m^3 s^{-1} with a

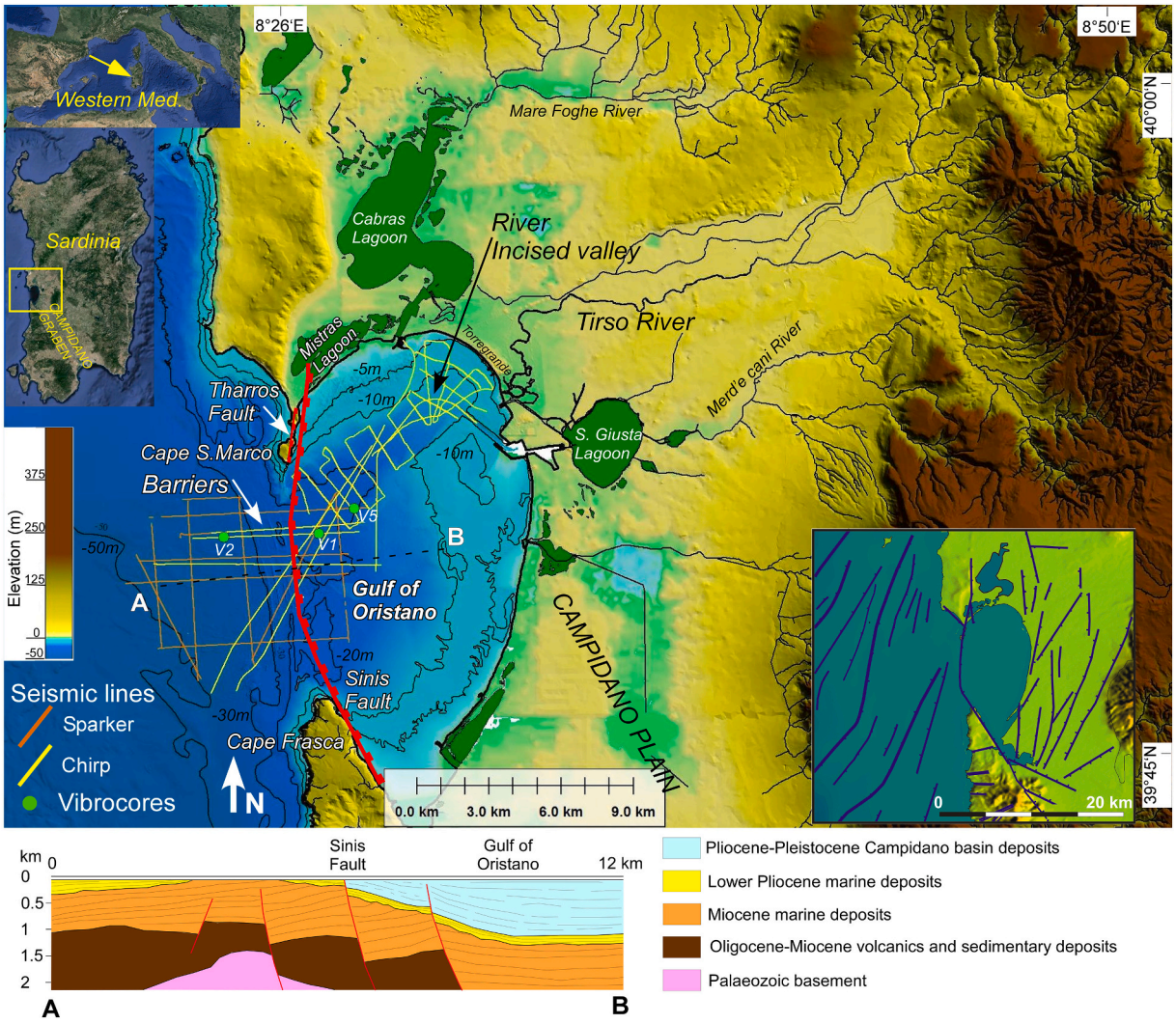

Fig. 1. Digital Elevation Model of the study area derived from SRTM 10 m (terrestrial area), and multibeam echosounder data (marine sector), showing the position of seismic lines and vibrocores collected in the marine sectors (from De Falco et al., 2015). The location of the study area (top- left corner) and a structural sketch (bottom-right corner) are reported. The position of the Sinis master fault at the entrance of the Gulf of Oristano is from Casula et al. (2001). The marine sectors not covered by multibeam data were interpolated from nautical maps. A-B: geological cross-section.

return periods of 2 and 50 years respectively (Mancini and Tilocca, 2007). Two other minor rivers, the River Mare e Foghe and the River Merd'e Cani, flow to the two major lagoons: the Cabras lagoon in the north and Santa Giusta lagoon to the south. The River Mar'e Foghe has a catchment area of 323 km^2 while the River Merd'e Cani is dry during part of the year and drains a restricted area of the Campidano plain.

Hydrodynamics in the Gulf of Oristano are mainly dominated by wind and wave action (Cucco et al., 2006). The astronomic tides in the area are of limited amplitude, with a range of ~20 cm (Simeone et al., 2014).

The dominant wind of the area is the Mistral, from the northwest, which comprises 70% of wind events with intensities higher than 10 m s^{-1} (Cucco et al., 2006). Maximum values of the vertically integrated current velocity, higher than 0.4 m s^{-1}, are reached when a Mistral wind of about 15 ms^{-1} forces the water circulation. Significant wave height is generally greatly reduced inside the Gulf, because of the shallow water depth. Wave energy, generated by Mistral winds, is at a maximum in the central and southern parts of the basin which are directly exposed to the Mistral wind wave action. On the other hand, lower values of significant wave height are found in the northern area where the wave energy is strongly attenuated by the sheltering effect of the S. Marco cape (De Falco et al., 2008).

Along the western Sardinian shelf, a typical Mistral wind storm with a return period of 1 year produces a significant wave height of 8 m, a peak period of 10 s and a peak wave direction of 308° (northwest), whereas the storms with a return period of 10 years are characterized by a significant wave height of 10 m and a peak period 11.5 s (De Falco et al., 2015b). Outside the Gulf the oceanographic setting is dominated by a surface current flowing southward, close to the western Sardinian shore with a noticeable stationary component.

3. Methods

3.1. Geophysics

A total of 126 km of very high-resolution seismic lines were acquired using a Chirp Benthos operating at 2.5–7 kHz, during two cruises (Fig. 1). Lines located at the Gulf entrance were acquired by the chirp sub bottom device hull-mounted on the R/V Urania of the Italian National Research Council in the year 2013. Lines located in the Gulf of Oristano, between the river mouth and the Gulf entrance were acquired with the pole-mounted transducer on a small boat of the Penisola del Sinis Isola di Mal di Ventre Marine Protected Area in the year 2017.

The conversion of two-way travel time to real depth was obtained

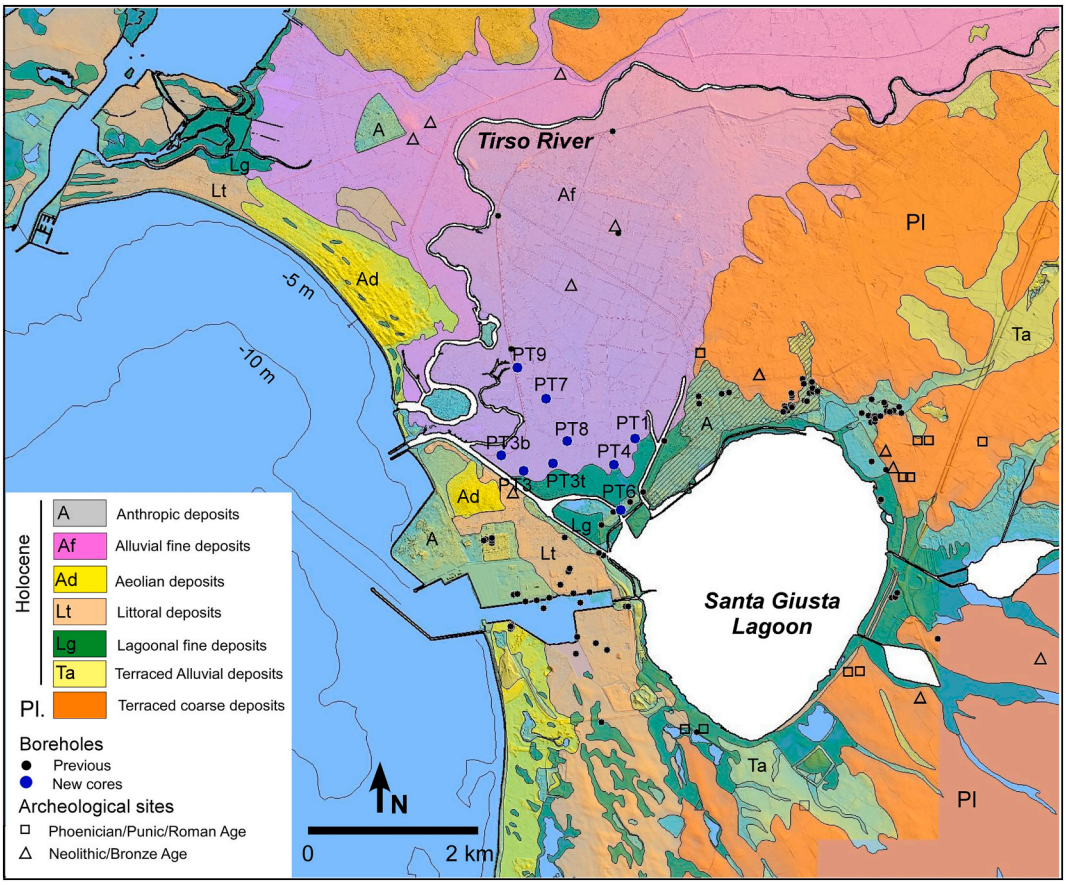

Fig. 2. Geological map of the coastal plain of the Tirso river with location of sampling points of the new cores collected for this study, previous boreholes available in the study area and distribution of archaeological sites.

assuming an average velocity of 1500 m s^{-1} below the sea floor. Chirp data allowed for a lateral resolution of 0.6 m and a vertical resolution of 0.5 m. All seismic data were processed in order to increase the signal/noise ratio using the software Geosuite. Our interpretation of the seismic stratigraphy was based on Mitchum et al. (1977).

Chirp data were integrated with previous seismic data collected at the Gulf entrance (Sparker operating at 0.8 kJ) and shown in a previous paper (De Falco et al., 2015a). Three vibrocores (V1, V2 and V5, Fig. 1) described in De Falco et al. (2015a), were used to calibrate the seismic units revealed by the new chirp data. Multibeam data derived from a different survey which were also reported by De Falco et al. (2015a). The position of seismic lines and vibrocores were obtained using a differential GPS system.

All geophysical data are available in the repository http://marinedata.cnr.it

3.2. Coring and sediment analysis

Preliminarily, >70 borehole descriptions were catalogued and analysed in order to provide a litho-stratigraphic reconstruction of the whole coastal plain (see Fig. 2 for the borehole locations). Based on this we planned the collection of 9 new cores (Fig. 2) in the sector between the Santa Giusta lagoon and the river, in an area with the presumably thicker Holocene sediments.

The new boreholes were drilled to a variable depth, down to 27 m, in order to collect the whole Holocene stratigraphic sequence that overlies the Pleistocene alluvial sediments. Elevations of the cores with respect to the current mean sea level were obtained with a DGPS-RTK survey (vertical approximation ±0.15 m).

In the laboratory, cores were described for a preliminary classification of lithofacies. Five cores (PT8, 27.5 m length, PT9, 27 m length, PT6, 20.4 m length, PT3bis, 10 m length, PT3ter, 10 m length) were sampled and analysed in detail. The PT8 core was sampled with a variable sample interval (0.1 m for the interval 0–10 m, 0.5 m for the interval 10–27 m); the PT9 and PT3bis cores were sampled at an interval of 0.5 m; PT6 and PT3ter cores were sampled at an interval of 1 m. Each core section was analysed for sediment grain size. Samples were wet sieved at 90 μm, after pre-treatment with H_2O_2, to separate the finer and coarse fraction. The former was analysed by a Galai CIS1 laser system, the latter by dry sieving (De Falco et al., 2015a). The muddy levels of the cores contained several shell layers which were sampled during core sampling. Additional shell samples were sampled during the grain size analysis. Furthermore, the muddy layers were analysed for water content and total organic matter by loss of weight at 110° (12h) and 550° (3 h) respectively.

Malacological remains collected and sieved from the sediment sampled from the cores were analysed to define the paleoecological conditions of the depositional environments. A first taxonomical identification process was followed by the taphonomical analysis of shell condition and traces (fragmentation, internal biofouling and bioerosional marks, marine erosion, predation bores). The ecological study of the different taphocoenosis highlighted the biofacies, improved the ecological definition of each lithofacies.

3.3. Dating and indicators of former relative sea level

Five samples from the PT8 core were collected for AMS ^{14}C radiocarbon dating, which was performed by Beta Analytic's laboratories. Four samples of the mollusc *Cerastoderma glaucum* were found in life position with both articulated valves; one sample was a shell of a

Mytilidae (Table 1). Radiocarbon data were calibrated using CALIB 8.2 (Stuiver et al., 2022). IntCal20 and Marine20 calibration method were applied according with what proposed by Di Rita et al. (2011). Local deviations of the marine reservoir effect were taken into account using a ΔR value of −137 ± 82, which is a mean of the value of the area including all the data available for the westernmost part of the Mediterranean sea. For all samples, the error associated with the measure of core elevation (0.15 m), the measure of depth in core (0.15 m) and the indicative range (IR, the elevation range over which an indicator forms, following Vacchi et al., 2016) was included in order to evaluate the vertical variability of former sea level position associated with each proxy. The age variability was computed using the 2σ ranges associated to calibrated radiocarbon data. The *Cerastoderma glaucum* used for dating were associated with molluscs like *Scrobicularia plana,* characteristic of estuarine intertidal conditions, and to seagrass fibers, of shallow marine environments. That association was also found in the present seabed of the Gulf of Oristano at ca. 2 m of depth (Como et al., 2008). This value was used as an IR according to the value attributed by previous authors to this proxy (Lambeck et al., 2011; Vacchi et al., 2016, 2018).

The new radiocarbon data were included in the datasets of dated relative sea level indicators during the last 9 ka, available for the Gulf of Oristano (De Falco et al., 2015a; Melis et al., 2017; Pascucci et al., 2018), and reviewed by Vacchi et al. (2018).

4. Results

4.1. The submerged incised valley

The stratigraphy of the TIV can be inferred by the interpreted seismic lines reported in Fig. 3-5. Seven seismic units were identified based on their external form, upper and lower boundaries and typical reflector configuration (Table 2). The seismic unit Ua is the basal unit that can be identified in the sparker lines offshore the Gulf of Oristano (Fig. 3). Its internal configuration is characterized by low-amplitude parallel reflectors, erosionally truncated at their upper contacts (Fig. 3). The unit Uc is characterized by high amplitude sigmoid and parallel reflectors, that downlap the lower boundary over the Ua. The Ua and Uc units are truncated by the surface S1 which has been represented as dashed red lines in Fig. 3. The unit U1 is characterized by medium amplitude reflectors, with wavy clinoform configurations, which downlap and onlap the lower boundary. The upper boundary is concordant with the uppermost reflectors. The maximum thickness is ca. 20 ms. Unit U1 infills the depression incised into the Ua and Uc units along the open shelf (Fig. 3). Units Ua, Uc and U1 are visible only in Sparker lines, whereas they are opaque in the chirp line (Fig. 4, Line 1).

Unit U3 was divided into two sub-units (U3a and U3b). U3a is characterized by high amplitude reflectors, U3b by medium amplitude reflectors. U3 reflectors onlap the lower boundary and toplap with the upper boundary. The maximum thickness of U3 is 18 ms. U3 infills the sector of the incised valley located inside the Gulf of Oristano (Figs. 4 and 5). U4 is characterized by prograding, high-amplitude reflectors. These reflectors downlap the lower boundary and toplap with the upper boundary. This unit is up to 10 ms thick and overlies the acoustic basement and is in lateral contact with the U3 unit. U6 represents a surficial drape with continuous parallel reflectors. U7 represent a thin unit which drape the valley infill in the Gulf of Oristano.

The seismic units were ground-truthed using sediment data from cores and surface sediment samples reported from previous studies (Francolini et al., 1990; De Falco et al., 2015a; De Falco et al., 2010; De Falco et al., 2008) (Table 2). Unit Ua can be correlated with marine fine-grained deposits dated to the Lower Pliocene (Francolini et al., 1990). No data are available for Unit Uc. Unit U1 was sampled in the vibrocore V5 and is composed of matrix supported pebbles and cobbles (De Falco et al., 2015a); unit U3a and U3b were sampled in the vibrocore V1 and are composed of organic-rich mud and to sandy mud respectively (De Falco et al., 2015a); Unit U6 are composed by sands to gravelly sands along the open shelf and at the gulf entrance, and muddy sands close to the river mouth (De Falco et al., 2008, 2010). Unit 7 is composed of sandy muds (De Falco et al., 2008).

The morphology of the TIV can be inferred from the bathymetric data and seismic cross sectional data shown in Figs. 3 and 5, where the Sinis master fault was also reported. In the Gulf the TIV is straight, ca. 2 km wide and underfilled by sediments (U3 unit) with the borders of the incision still visible at the seabed. The flanks are 3°to 6° steep (Fig. 5).

The valley changes its morphology when it crosses the Sinis master fault. Offshore the Gulf, the incised valley does not show morphological evidence at the seabed and is clearly visible only in the seismic sparker lines as a wholly-filled valley which incises the Ua and Uc seismic units (Fig. 3) and is filled by the U1 unit, forming a steep-sided (12° to 17°) narrower and embedded valley ~0.5–0.7 km wide and ~ 15 m deep. Westward, the valley changes direction and is directed to the south. Here the embedded valley widens (>1 km) and is filled by the U1 seismic unit and draped by the U6 unit (Fig. 3).

Along the TIV, the depth of the valley incision ranges from 80 ms (60 m below present sea level) in the more distal section (Fig. 3, section GH), 75 ms (56 m b.p.s.l.) at the Gulf entrance (Fig. 3, section AB), 45 ms (33 m b.p.s.l.) in the back barrier sector (Fig. 4, Line 1) and 35 ms (26 m b.p.s.l.) in the proximal sector inside the Gulf of Oristano (Fig. 4, Line 2).

4.2. The coastal plain

The stratigraphic correlations between the core profiles along two transects are reported in Fig. 6, based on the detailed core descriptions reported in the Supplementary Materials (Fig. S1 and S2).

The first transect is parallel to the present-day shoreline and connects cores PT9, PT7, PT8 and PT6 (Fig. 6 and Fig. S1), which intersected the thicker succession of the incised valley fill. Hereafter all along core depths are reported in meters below the present sea level.

The cores PT9 and PT8 were drilled down to a depth of 26 m and showed a similar stratigraphy. The lowest part of the cores were composed of rounded heterometric pebbles of different lithologies in a sandy matrix (Unit P, Fig. 6). This is covered by a terrigenous deposit characterized by silty sands (Unit D2 in PT9 and D in PT8, Fig. S1).

Table 1
AMS 14C radiocarbon age dating of shells sampled along PT8 core (see S1 for core description). The radiocarbon ages were calibrated using CALIB 8.2 (Stuiver et al., 2022).

Core	Depth in core m	Elevation p.s.l. m	Sample description	^{13}C age Years BP	δ^{13}C (‰)	Calibration Dataset	Cal. Age (2σ) Years BP
PT8	6.1	5.6	*Cerastoderma glaucum*	4400 ± 30	0.7	Marine20	4617 ± 266
PT8	6.7	6.2	*Cerastoderma glaucum*	4410 ± 30	−0.4	Mixed Marine/ NoHem (98% Marine)	4639 ± 258
PT8	9.3	8.8	*Cerastoderma glaucum*	5110 ± 30	−0.4	Mixed Marine/ NoHem (98% Marine)	5498 ± 235
PT8	10.1	9.6	*Cerastoderma glaucum*	5700 ± 30	0.6	Marine20	6128 ± 230
PT8	19.6	19.1	*Mitylidae*	7650 ± 30	3.6	Marine20	8146 ± 223

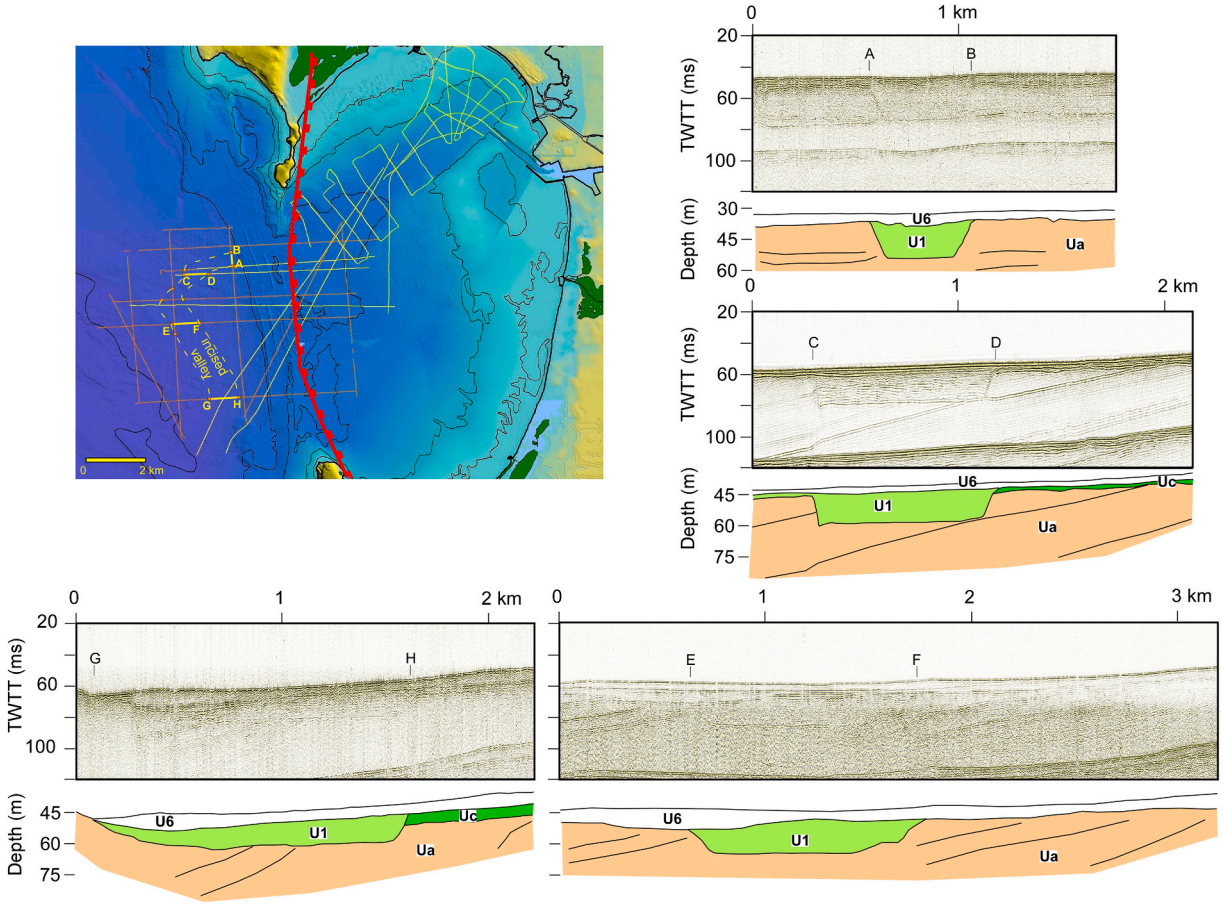

Fig. 3. Raw and interpreted high resolution seismic profiles (sparker source) of the sector offshore the Gulf of Oristano. The pathway of the TIV interpolated from the seismic lines is shown.

The overlying Unit C4 (~19–23 m) is a grey muddy deposit, with an organic matter content of ~8–10%. Abundant *Ostrea edulis* valves, *Cerastoderma, Chlamys,* Mytilidae and bioclastic fragments (mainly shattered Cardiidae and Ostreidae shells) and echinoderm spines attest to the prevailing marine conditions during deposition. This unit is 4.6 m thick in PT8 core, whereas in core PT9, Unit C4 is covered at 22 m by a 3 m-thick deposit (Unit D1, 18.9–22 m) of sands with wood remains and no marine fauna. This Unit D1 is characterized by one meter of ochraceous silty sands covered by alternating silty ochraceous layers and grey silty sands bearing angular quartz fragments. The top of D1 contains shell fragments clearly related to the overlying deposit.

A layer of shell debris 0.2 m-thick is present in both cores at a depth of 19 m and is composed of *Ostreidae*, *Mytilidae, Vermetus* and *Chlamys* fragments rich in *Serpulidae* remains in a muddy matrix. A *Mytilidae* shell from this layer from core PT8 has been dated at 8146 ± 223 cal y BP (Table 1).

Unit C3 (~12–19 m) comprises a blackish muddy interval rich in mica, with an increasing in organic matter content with stratigraphic height (from ~5% to ~10%, Fig. S1). Repeated thin intercalations of tiny shells and fragments of *Cardiidae* and *Tellinidae* are common. Most of the taphocoenosis are characterized by the presence of shells of *Corbula gibba* (a pioneer and opportunist species) shells in living position, abundant Tellina sp. (only in core PT8) and rarer shells of *Lentidium mediterraneum*, an estuarine shallow water species. In the PT9 core the lower half of the unit (up to 15.0 m) is also characterized by the occurrence of seagrass fibers, *Chlamys, Cardiidae* and *Veneridae* shell fragments and *Dentalium*. In the upper half, the first occurrence of *Cerastoderma glaucum* in life position are found.

A finer deposit at the top of the unit C3 (11.3–11.8 m) is present on both cores PT8 and PT9 and is characterized by reddish horizons and thin calcrete layers (PT9) and rare, very fine *Cerastoderma glaucum* fragments (PT8).

This passes upward to the unit C2 (~6.5–11.5 m) that consists of a dark grey mud, rich in organic matter (~10%), with intercalated layers of *Cerastoderma glaucum* valves with several specimens in living position. The intervals between 9.5 and 10 m are characterized by abundant valves and fragments of *Cerastoderma glaucum, Scrobicularia plana*, *Anomia ephippium* and Tellinidae. In the core PT8, *Cerastoderma glaucum* in living position were dated at 6128 ± 230 cal years BP (10.5 m) and 5498 ± 235 cal years BP (9.3 m). The intervals between 6.5 and 8 m are characterized by a progressive increase in seagrass fibers, small *Rotalids* forams and ostracods.

Unit C1 (5.1–6.4 m) is characterized an by increased silty fraction and by the abundance of *Posidonia* seagrass fibers, egagropiles, *Cerastoderma glaucum* and *Bittium reticulatum* and Tellinidae. In core PT9, at 5.4 m, a mass of egagropiles seagrass balls with *Bittium* sp., *Loripes lucinalis* and Tellinidae fragments occur. In core PT8, a shell from 6.7 m has been dated at 4639 ± 258 cal years BP.

A further unit C0 (6.7–5.4 m) was recognized in core PT8, and it comprises a dark grey mud with white mica, characterized by *Cerastoderma* and *Scrobicularia* valve and fragments mixed with rare charcoals elements. Ostracods and foraminifera are absents. *Corbula gibba*, a typical opportunist species occurs in the bottom layer. A layer at 6.1 m was dated at 4617 ± 266 cal years BP and contained a *Scrobicularia plana* shell in living position (Fig. S1). An erosive surface caps the deposits of unit C. A sharp change in lithological facies characterizes the following deposits (Unit B, ~0.5–5.4 m), which are composed by sandy gravels and gravelly sands with biotite and insect cuticles.

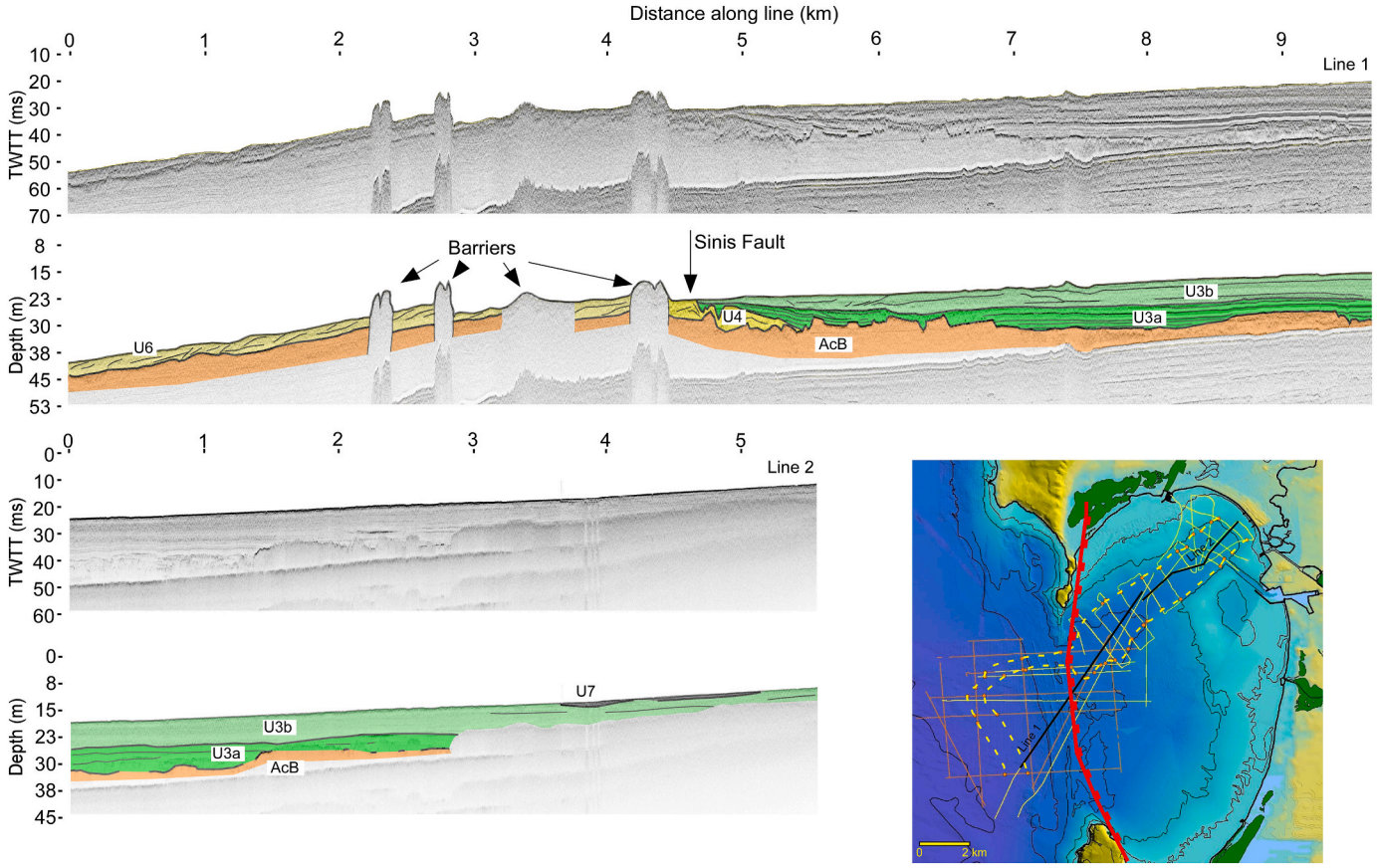

Fig. 4. Raw and interpreted very high resolution seismic profiles (Chirp – 3.5 kHz) collected along the axis of the incised valley and through the Gulf entrance. The pathway of the TIV interpolated from the seismic line is shown.

The top of the cores (Unit A, 0–2 m) comprises muddy deposit with relative low organic matter content (~4%) and without shell fragments. At 0.8 m pedogenetic features occurs.

The along core sortable/non sortable ratio (Mccave and Hall, 2006) is described below. The S/NS ratio is the ratio between two grain size fractions (sortable fraction is equivalent to 8–63 μm, non sortable fraction is <8 μm) and is a proxy of the hydrodynamic energy of the depositional environments. The S/NS is >1 in the lower part of the C4 deposits which were deposited during the initial phase of marine transgression. S/NS decreases in the range 0.5–1 in unit C3. The lowest values (<0.5) were recorded in the unit C2. S/SN increases again in C1 (Fig. S1).

Core PT6 (Fig. 6 and Figue S1) was drilled down to a depth of 20.4 m and showed a stratigraphic succession similar to PT8 and PT9 cores with a more condensed succession (c.a 14.5 m) of Holocene sediments.

The second transect connects PT3bis to PT1 cores (Fig. 6 and Fig. S2 in supplementary materials). Along the western side of the transect, toward the present day shorelines, cores PT3bis, PT3 and PT3ter sampled the Pleistocene alluvial sediments (P in Fig. 6) at a depth of 6–7 m. Here the Holocene succession is represented by gravelly to muddy sands with shell fragments (B1). To the east, floodplain deposits (B) overlie the coastal deposits (core PT3 and PT3ter). The stratigraphic succession terminates with muds and muddy sands (A). The second transect crosses the first transect at the core PT8 previous described.

4.3. Age model and relative sea-level variations

The age model of the incised valley fill was inferred from the radiocarbon data collected along the muddy deposits of PT8 core (C1 to C0 facies, Table 1) and compared with other radiocarbon data available in the area. All data are plotted in Fig. 7, where the position of each RSL indicator, with vertical (sea-level) and horizontal (age) ranges, deriving from the various data sets are reported. RSL data show a rapid rise in sea level up to ~6–7 ka followed by reduction in the rate of sea level rise, according to the previous published sea level curves (Vacchi et al., 2016; Lambeck et al., 2011). However, the RSL proxies are quite scattered and it is not possible to infer small variations (magnitude of meters) in the rate of the sea-level rise rate occurred over the last 9 ka. Dated strata in core PT8 were used to evaluate the sedimentation rate, yielding a value of 4.7 mm year^{-1} from 8.2 to 6.1 ka (mainly corresponding to the C3 unit), which decreased to 2.6 mm year^{-1} from ~6 to ~4.6 ka (corresponding to C2, C1 and C0 units).

5. Discussion

5.1. Interpretation of depositional environments

The interpretation of depositional environments of seismic and sedimentary units is reported in Fig. 8, where a schematic longitudinal profile of the stratigraphic stacking pattern of the TIV is represented. The sector of the valley outside the Gulf of Oristano was filled by unit U1, which is composed of pebbles and cobbles in a sandy matrix (De Falco et al., 2015a). Unit U1 is interpreted as alluvial deposits which fill the mid-outer sector of the valley in subaerial conditions. Alluvial deposits have been reported at the base of the filling of the incised valleys in previous studies (Green et al., 2013; Maselli et al., 2014; Dladla et al., 2019).

An overstepped barrier system formed at the Gulf entrance at a depth of ~36 m to 16 m (Fig. 4) following the high rate of the sea-level rise (~9 mm y^{-1}, Vacchi et al., 2021, Fig. 7) (De Falco et al., 2015a). The seismic unit U4, characterized by landward prograding reflectors is interpreted as washover deposits of the back-barrier sector (Shan et al.,

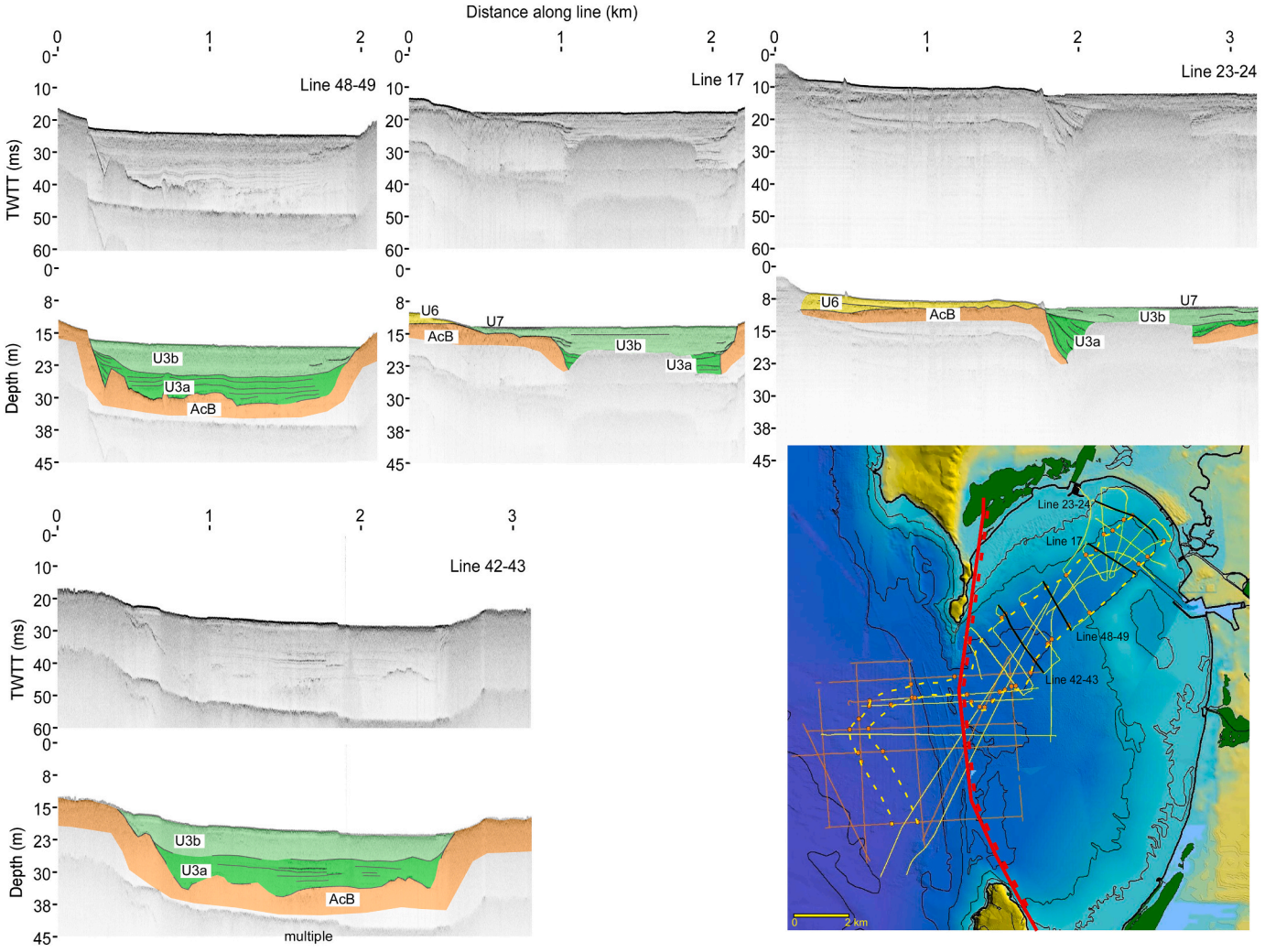

Fig. 5. Stratigraphic cross-section of the TIV derived from very high resolution seismic profiles (Chirp – 3.5 kHz).

2016; Mellett et al., 2012). The seismic unit U6, characterized by seaward prograding reflectors is interpreted as the shoreface deposits of the barrier system (De Falco et al., 2017; Pascucci et al., 2018; Salzmann et al., 2013). The seismic units U3a, composed by organic-rich mud, was interpreted as back-barrier lagoonal deposits (Fig. 8). This is keeping with similar observations of back-barrier fills from around the word (Dladla et al., 2022; Green et al., 2022).

After barrier drowning, a marine environment prevailed in the TIV with the deposition of unit C4, containing typical marine fauna (Fig. 8). The shell layer at ~19 m, dated 8.2 ka BP, could be related to a reduction of sediment supply with the presence of articulated valves excluding that this layer's deposition as a residual lag. A shell horizon (or condensed bed) reflects the maximum rate of relative sea-level rise (sensu Catuneanu, 2006). According to Vacchi et al., 2021, this event is related to a deceleration in the rate of relative sea level rise during the interval ~ 7–8.5 ka BP. The presence of the shell layer can be tentatively interpreted as due to a local reduction of sediment supply rather than an increase of the rate of the relative sea-level rise.

The overlying muddy deposit (Unit C3), reveals the presence of pioneer and opportunist species which denotes stressed estuarine conditions, with intense fluvial sediment supply, in a shallow inner bay. The sedimentation rate which can be inferred from core PT8 for C3 unit is 4.7 mm year^{-1} (over a time interval ranging from 8.2 ka to 6.1 ka) and can be related to a period of more intense precipitations and high sediment supply which was documented in the Mediterranean region (Zhornyak et al., 2011) due to the fluctuation of the African monsoon region. This climatic phase was related to the deposition of Sapropel S1 in the eastern Mediterranean (Zanchetta et al., 2007). The increase in sediment supply linked, to climate forcing during this wet period, was also documented in the infill of the Manfredonia incised valley in the Adriatic Sea (Maselli and Trincardi, 2013; Maselli et al., 2014). During this period the rate of sea-level rise rate was estimated to decrease from ~6 mm y^{-1} to ~2 mm y^{-1} (Vacchi et al., 2021), which is a value similar to the sedimentation rate. The system kept in pace with rising sea level and thus aggraded with a uniform and monotonous series of muds, analogously to what is described for this exact scenario for many of the estuaries of the SE African coastline (Cooper, 1993; Cooper et al., 2012). During this phase, the valley was filled by ~7 m of estuarine muds forming the C3 unit.

The seismic Unit 3b can be considered coeval with Unit C4 and C3. The basal level of unit U3b was dated 8.7 ka while the transition between C4 and C3 is dated 8.2 ka. Unit U3b can be interpreted as the TIV infill in the Gulf of Oristano in marine/estuarine conditions, in analogy with units C4 and C3.

The overlying unit C2 Unit, with the organisms typical of brackish sheltered environment, attests to a lagoon formation and consequently the formation of a bar or barrier to seaward during ~6.1–5.5 ka (B1, Fig. 8). The progressive change in biofacies change from C2 to C1 (~4.5 ka) reveals an increasing marine influence and a gradual transition to a more open marine environment in proximity of seagrass meadows, as

Table 2
Description of seismic units interpreted from the seismic reflection profiles and related lithofacies.

Seismic units	Geometry	Upper/Lower Boundaries	Reflector Configuration	Lithofacies/ Calibration
Ua	Base Unit	Erosional Truncation/ n. d.	Parallel, top discordant, low amplitude	Mud (Francolini et al., 1990)
Uc	Wedge	Erosional truncation /downlap	Sigmoid/Parallel, continuous, high amplitude	No Data
U1	Fill	Concordance/ Onlap-Downlap	Wavy clinoforms, continuous, medium amplitude	Matrix supported pebbles and cobbles / Core V2 (De Falco et al., 2015a)
U4	Sheet/ wedge	Toplap/ Downlap	Prograding parallel/Sigmoid Oblique, continuous, high amplitude	Fine sands to matrix supported granules and pebbles / Core V5 (De Falco et al., 2015a)
U3	Fill	Concordance-Toplap/Onlap	Parallel/Sigmoid, continuous, high (U3a) to medium (U3b) amplitude	Organic-rich mud to sandy mud / Core V1 (De Falco et al., 2015a)
U6	Drape	n.d./ Concordance-Onlap	Parallel, continuous, high amplitude	Muddy Sand to gravel / Cores V1, V5, V2 (De Falco et al., 2008, 2010, 2015a)
U7	Drape	//	//	Sandy mud to mud / Grab samples (De Falco et al., 2008)

denoted by the abundance of seagrass balls (egagropiles) in core PT9 associated with a seagrass meadow taphocoenosis (Fig. S1). The interval C2-C1 is characterized by a strong reduction in the sedimentation rate (2.6 mm year^{-1}, over a time period from 6.1 ka to 4.6 ka), attesting to a reduction in sediment supply. The rate of sea-level rise decreased from ~2 mm y^{-1} to ~0.5 mm y^{-1} (Vacchi et al., 2021), thus allowing the formation of coastal systems.

The barrier-lagoon system (B1- C2-C1, Fig. 8) developed over a time interval from 6.1 to 4.6 ka which can be correlated with the cold phases known as "Sahara Aridity" or the Post Late Neolithic arid phase (Walsh, 2014), during which the coldest period after the Younger Dryas occurred (Perry and Hsu, 2000). This oscillation marks the end of the Atlantic climate regime, and the beginning of the Sub-Boreal (Blytt- Sernander Sequence, Rydin and Jeglum, 2013). In particularly two climatic dry events are well documented in the Mediterranean Sea during this period, 5.2–5.6 ka dry event (Zanchetta et al., 2007) and the worldwide 4.2 ka event (Zanchetta et al., 2016). Those dry events could be related to the reduction of sediment supply in the unit C2-C1, and the formation of barrier lagoon system following the reduction in the rate of sea-level rise.

After 4.6 ka, the seaward progradation of the alluvial facies and associated environments occurred with the deposition of coarse alluvials over an erosional surface, at 6.1 m in PT8 and PT9 cores, which signalled the termination of marine sedimentation (Fig. 8, S1). This phase could be tentatively related to a phase of sea-level still stand (or possible drop) based on an the analogue of adjacent Mistras lagoon (Pascucci et al., 2018). Specifically, this interpretation is consistent with the presence of a non-depositional hiatus between 6.0 and 3.0 ka over an erosional surface which was recorded in the adjacent Mistras barrier-lagoon and was associated with a relative sea level drop occurred during this cold period (Pascucci et al., 2018).

The strong seaward progradation of the alluvial facies after 4.6 ka was recorded along the whole valley as shown by the paleo-environmental reconstruction of the northern sector of Tirso river plain made by Melis et al. (2017) which reported a progradation of alluvial deposits occurred between 5.5 and 2.9 ka BP over lagoonal and marine deposits.

The depositional sequence of the TIV is also consistent with the parasequence architecture of the Po river plain (Amorosi et al., 2017) which was related to millennial-scale relative sea level fluctuations. Particularly, coastal progradation of the Po river plain started from 7 ka (parasequences 4–8, Amorosi et al., 2017) which can be correlated to the date of forming of B1-C2 barrier lagoon system.

Finally, the formation of the barrier B0 (Fig. 8) can be related to the further rise in the sea level up to the present-day position. This event was not dated in our cores and could be tentatively related to maximum inland marine Holocene ingression which occurred at 2.5 ka BP according to Pascucci et al. (2018).

5.2. *Morphology and sedimentary infill of the incised valley related to the tectonic setting*

The TIV is the result of a single event of incision and infill related to the last eustatic cycle and can be classified as a simple incised valley (sensu Zaitlin et al., 1994). Most of the incised valleys studied worldwide, in passive margins, were classified as compounds because several episodes of valley incision and filling were recognized (Thomas and Anderson, 1994; Zaitlin et al., 1994; Gensous and Tesson, 1996; Greene Jr. et al., 2007; Tesson et al., 2011; Dladla et al., 2019).

Examples of single downcutting-event producing incised valleys are less frequent (Chaumillon et al., 2008; Crockett et al., 2008; Maselli and Trincardi, 2013; Qiu et al., 2019), and were in some cases related to an interval of dramatically increased discharge, typically related to ice melting (Lericolais et al., 2003; Gupta et al., 2007; Thieler et al., 2007). In our case the TIV was not conditioned by ice melting because glaciers were not present in the catchment basin during the last glaciation.

An evolutionary model of the TIV can be inferred from the geomorphological and stratigraphic data (Fig. 9). Typically, the valley deepening occurs during accelerated relative sea-level fall and valley broadening occurs during reduced rates in sea level fall rate or rise (Martin et al., 2011). During the incision stage, valleys act as a corridor for sediment by-pass with the predominance of erosive processes (Blum et al., 2013).

The evolution of the TIV was strictly related to the geological setting of the Gulf of Oristano and western Sardinian shelf. The Gulf entrance corresponds to the Sinis main fault (Fig. 1) delimiting the Campidano Graben (Casula et al., 2001). The Sinis fault is a normal fault which lowered the eastern block (Cocco et al., 2013; Casula et al., 2001) and acts as a threshold separating areas with abrupt changes of geological and geomorphological conditions. Outside the Gulf, westward, the TIV cut early Pliocene marine deposits. The rollover of the horst-block associated with the fault causes the seabed, in this sector, to slope more steeply (0.3–0.5°). Inside the Gulf, eastward, the seabed is flatter (0–0.2°) and the TIV cut into Pleistocene alluvials. This threshold corresponds to a change in the incised valley morphology. Outside the Gulf the valley is narrower (~0.5–1 km) with steeper flanks (~12°-17°) whereas inside the Gulf the valley widens up to 2 km with less steep flanks (~3°-6°). This trend is opposite to the main common morphological features described for the incised valleys, which normally enlarge basinward (Martin et al., 2011) evolving in a funnel-shape incision.

Our interpretation of the evolution of the valley is that the presence of areas with different slopes and erodibility of the substrate, along the path of the valley, has conditioned its evolution in relation to the relative

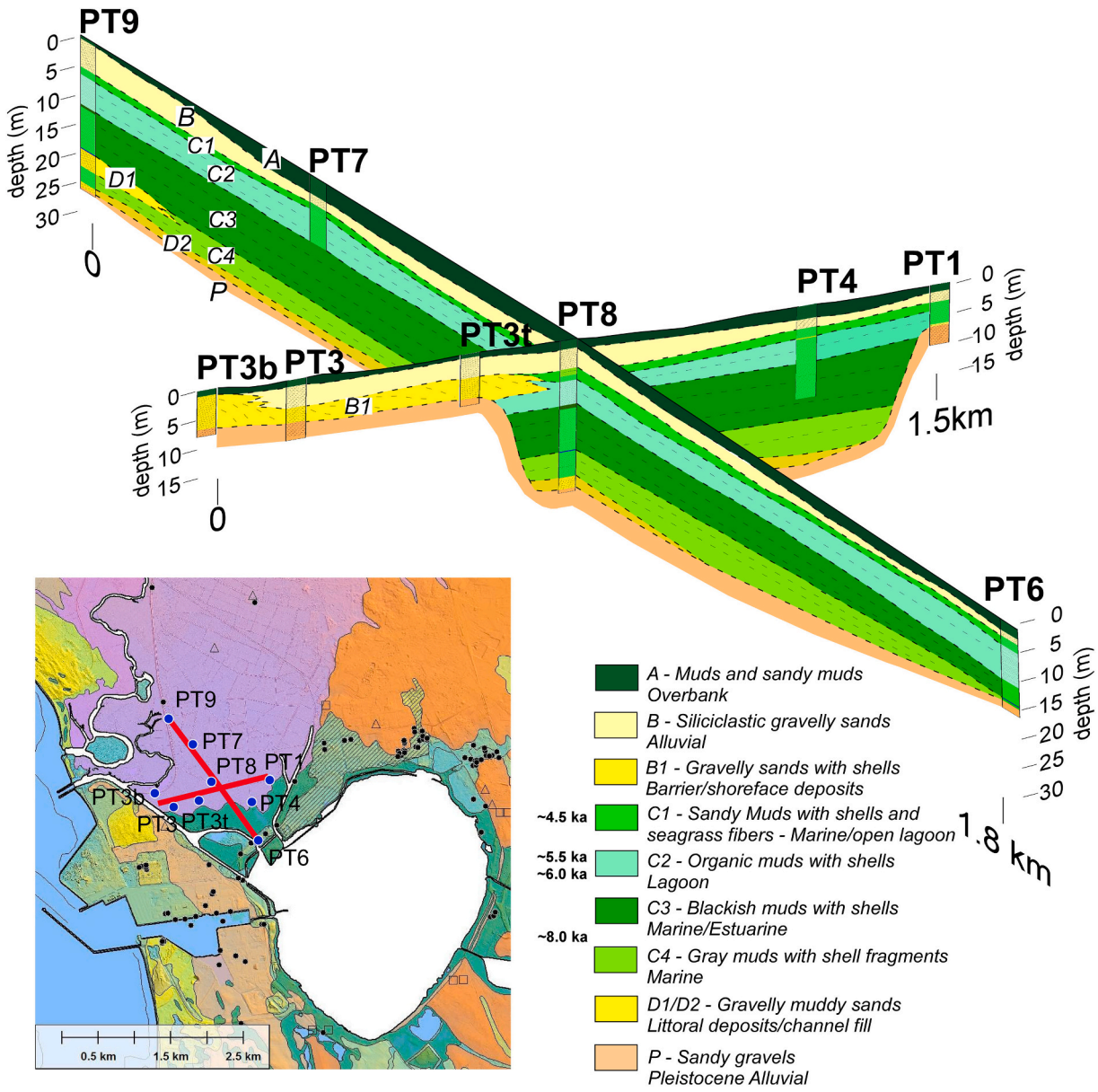

Fig. 6. Stratigraphic correlations among the core logs collected in the coastal plain (see Supplementary Materials from detailed core descriptions).

changes in the sea level. In particular, the prolonged still standing preceding each of the MWPs 1a and 1b (Liu et al., 2004) would allow for lateral adjustment in the proximal areas during an overall transgressive regime. This flatter zone would condition the meandering and broadening of the valley by lateral incision. The outer valley would not get to experience this as this area would be drowned more quickly because the seabed is steeper and is subject to harder geology that makes lateral adjustment more difficult (Gomes et al., 2016). It has been shown that valleys in soft lithologies widen downstream twice as fast as valleys in resistant lithologies, due to the erosional mechanisms of valley widening (Langston and Temme, 2019).

The proposed evolutionary model for TIV is analogous to that proposed by Gomes et al. (2016) for the incised valley of the Assu along the Brazilian equatorial shelf. The Assu valley is similarly characterized by an anomalous narrowing toward the outer shelf due to the presence of faults crossed by the valley. The presence of faults along the path of the incised valley leads to a variation in the geology of the bedrock (Gomes et al., 2016).

It is not still clear if late Quaternary tectonics could be active during valley formation, with a relative drop of the eastern sector. Sardinia is generally considered stable since MIS 5 (Antonioli et al., 2015). However, a recent study highlighted a tectonic offsetting of Pleistocene aeolianite, dated 82 ± 9 ka, along the Tharros fault located in Cape San Marco (Fig. 1) (Cocco et al., 2019). We cannot exclude that vertical movement along the Sinis fault could have occurred during valley formation, thus contributing to the formation of the sill at the Gulf entrance.

The geological inheritance and the oceanographic setting also conditioned the sedimentary environments along the valley west and east of the structural threshold at the Gulf entrance. Outside the Gulf, the shelf is exposed to stronger waves and currents driven by dominantly westerly winds (Cucco et al., 2006; De Falco et al., 2015b). Here the valley was mainly filled by coarse alluvial sediments and there are not fine-grained deposits along the shelf. Finer sediments were likewise dispersed to the deeper areas due to the strong wave and currents. Wave hydrodynamics and longshore currents favoured the formation of the barrier system at the Gulf entrance. When the sea level reached the Gulf entrance, a coastal system developed with a series of parallel barriers

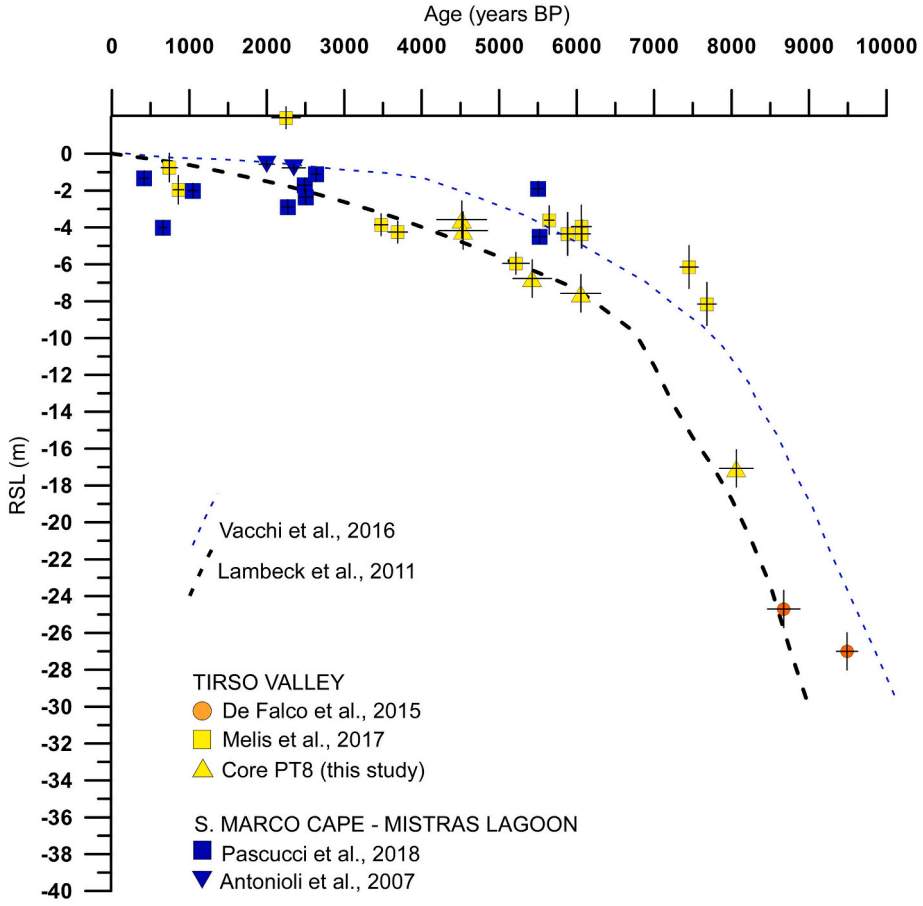

Fig. 7. Index points in the Gulf of Oristano, coupling data from PT8 core with data from previous studies. Vertical lines for each point represent the elevation errors associated with the measure of core elevation, depth in core and indicative range (IR, the elevation range over which an indicator forms, following Vacchi et al., 2016). The horizontal lines represent the age variability (2σ ranges) associated with the calibrated radiocarbon data. The relative sea level curves are also reported.

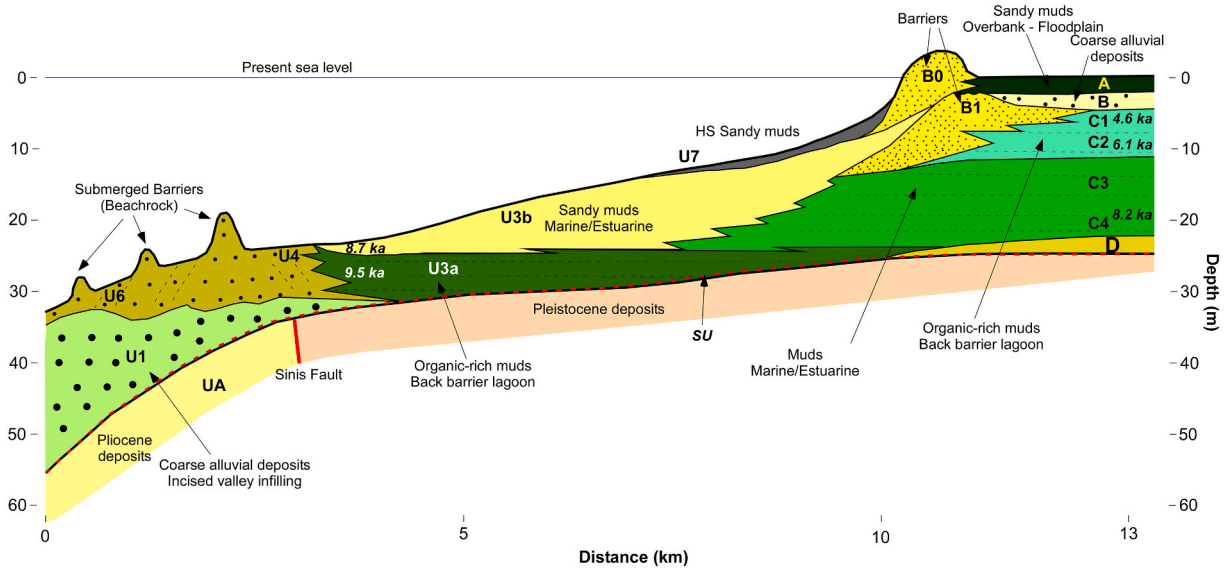

Fig. 8. Schematic longitudinal section of the Tirso River Incised Valley, from the coastal plain to the barriers at the entrance of the Gulf of Oristano. SU = subaerial unconformity surface.

located at 18 m/ 37 m below the present sea level (Fig. 4) (De Falco et al., 2015a). Those barriers enclosed a lagoon which was progressively filled by lagoonal and estuarine sediments. When the sea level was at the Gulf entrance (approximately at a depth of ~20 m b.p.s.l), the river mouth was located inside the present-day alluvial plane. With a further rising of the sea level, the barriers were drowned and the incised valley was filled by estuarine sediments in the area more proximal to the river mouth and by shoreface sediments in the more distal area inside the Gulf

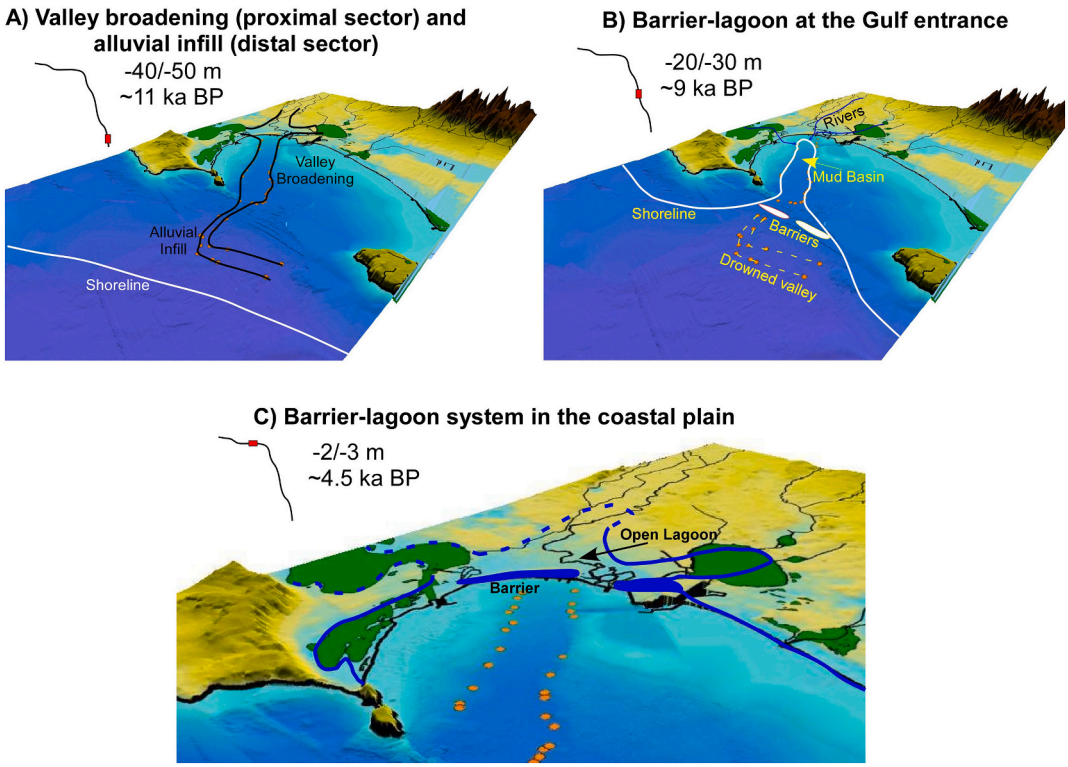

Fig. 9. Cartoon showing the idealized geomorphological evolution of the valley during the post-glacial sea level rise.

(Fig. 8). Coastal systems in proximity of the present-day shoreline developed when sea level approached to the highstand (~6 ka).

6. Conclusions

The Tirso Incised Valley (TIV), in Western Sardinia is an example of a simple incised valley controlled by sea-level changes and inherited geological constraints, such as the presence of a major fault (the Sinis fault) delimiting the western border of the Campidano graben. In fact, this structural boundary marks an abrupt change in substrate lithology and seabed slope, and causes a consequent change of TIV morphology, getting from narrow within the Pliocene formations, to wide inside the Gulf, where the TIV incises Pleistocene alluvial deposits in the flatter bay of the Gulf of Oristano; this threshold also controlled the nature of valley infill.

The stratigraphic record describing the TIV evolution during the Holocene begins with alluvial sediments which filled the valley during the initial phase of the latest sea level rise. At ~9 ka the sea level raised the Gulf entrance. Here, a series of barriers formed closing a lagoon with a mud basin in the valley. The lagoon/marine and estuarine infill of this sector was modulated by the presence of the barriers at the gulf entrance, by the rate of sea level rise, and by the sediment supply, which was in turn related to multi-centennial-scale Holocene climate events. In particular, absolute dating denoted a reduction in sediment supply at 8.1 ka, high sedimentation rates during valley infilling related to the humid period at 8–7 ka BP and lower sedimentation rate related to the dry period consequent to the cold phase at 6–4 ka BP. During the latter, a decrease in the rate of sea level rise allowed for the formation of coastal systems. After 4.5 ka BP a strong progradation of the alluvial deposits occurred, related to a phase of sea level stillstand, or possible drop, correlated to an analogous regressive phase in the adjacent Mistras lagoon. A further sea level rise allowed for drowning of the alluvial plain and the formation of the present-day barrier system.

Supplementary data to this article can be found online at https://doi.org/10.1016/j.margeo.2022.106885.

Data availability

Bathymetric data are available at EMODnet Bathymetry Consortium (2020): EMODnet Digital Bathymetry (DTM), doi:10.12770/bb6a87dd-e579-4036-abe1-e649cea9881a. Seismic data (routes of Chirp SBT and single channel Sparker line) are available at http://sk.oristano.iamc.cnr.it/maps/378. Raw seismic data are available as upon request to giovanni.defalco@cnr.it. The seismic data and grain size data of sediment cores were submitted to the PANGEA data publisher (waiting for DOI).

Declaration of Competing Interest

The authors declare that they have no known competing financial interests or personal relationships that could have appeared to influence the work reported in this paper.

Acknowledgements

We acknowledge G. Stanghellini (CNR ISMAR Bologna) for the support to seismic survey. The work has been funded with grant Legge Regionale 7/2007 Project: “Interazioni tra uomo e ambiente nell’evoluzione del paesaggio costiero antico della Sardegna”, funded by Regione Autonoma della Sardegna (RAS), Assessorato della Programmazione, Bilancio, Credito e Assetto del Territorio (Base Research Project, L.R. 7 agosto 2007, n. 7, Annualità 2013, Resp. Carla Del Vais). Partial fund has been provided by the project RITMARE ICM Golfo di Oristano – Linea Dati (Res. Giovanni De Falco), funded by Italian Ministry of Research and Education.

References

Allen, G.P., Posamentier, H.W., 1993. Sequence stratigraphy and facies model of an incised valley fill: the Gironde Estuary, France. J. Sediment. Res. 63, 378–391.
Amorosi, A., Bruno, L., Campo, B., Morelli, A., Rossi, V., Scarponi, D., Hong, W., Bohacs, K.M., Drexlercet, T.M., 2017. Global sea-level control on local parasequence

architecture from the Holocene record of the Po Plain, Italy. Mar. Pet. Geol. 87, 99–111.
Anthony, E.J., Oyédé, L.M., Lang, J., 2002. Sedimentation in a fluvially infilling, barrier-bound estuary on a wave-dominated, microtidal coast: the Oue´me´ River estuary, Benin, west Africa. Sedimentology 49, 1095–1112.
Anthony, E.J., Marriner, N., Morhange, C., 2014. Human influence and the changing geomorphology of Mediterranean deltas and coasts over the last 6000 years: from progradation to destruction phase? Earth Sci. Rev. 139, 336–361.
Antonioli, F., Anzidei, M., Amorosi, A., Lo Presti, V., Mastronuzzi, G., Deiana, G., De Falco, G., Fontana, A., Fontolan, G., Lisco, S., Marsico, A., Moretti, M., Orrù, P.E., Sannino, G.M., Serpelloni, E., Vecchio, A., 2015. Sea-level rise and potential drowning of the Italian coastal plains: flooding risk scenarios for 2100. Quat. Sci. Rev. 2017 (158), 29–43.
Blum, M.D., Martin, J., Milliken, K., Garvin, M., 2013. Paleovalley systems: insights from Quaternary analogs and experiments. Earth Sci. Rev. 116, 128e169. https://doi.org/10.1016/j.earscirev.2012.09.003.
Burger, R.L., Fulthorpe, C.S., Austin Jr., J.A., 2001. Late Pleistocene channel incisions in the southern Eel River Basin, northern California: implications for tectonic vs. eustatic influences on shelf sedimentation patterns. Mar. Geol. 177, 317–330.
Cartelle, V., García-Moreira, I., Martínez-Carreño, N., Muñoz Sobrino, C., García-Gil, S., 2022. The role of antecedent morphology and changing sediment sources in the postglacial palaeogeographical evolution of an incised valley: the sedimentary record of the Ría de Arousa (NW Iberia). Glob. Planet. Chang. 208, 103727.
Casula, G., Cherchi, A., Montadert, L., Murru, M., Sarria, E., 2001. The Cenozoic grabens system of Sardinia: geodynamic evolution from new seismic and field data. Mar. Pet. Geol. 18, 863–888.
Catuneanu, O., 2006. Principles of Sequence Stratigraphy. Elsevier, Oxford (375 pp.).
Chaumillon, E., Proust, J.-N., Menier, D., Weber, N., 2008. Incised-valley morphologies and sedimentary-fills within the inner shelf of the Bay of Biscay (France): a synthesis. J. Mar. Syst. 72, 383–396.
Cherchi, A., Mancin, N., Montadert, L., Murru, M., Putzu, M.T., Schiavinotto, F., Verrubbi, V., 2008. The stratigraphic response to the Oligo-Miocene extension in the western Mediterranean from observations on the Sardinia graben system (Italy). Bull. Soc. Geol. Fr. 179 (3), 267–287.
Cocco, F., Andreucci, S., Sechi, D., Cossu, G., Funedda, A., 2019. Upper Pleistocene tectonics in western Sardinia (Italy): insights from the Sinis peninsula structural high. Terranova. https://doi.org/10.1111/ter.12418.
Cocco, F., Funedda, A., Patacca, E., Scandone, P., 2013. Plio-Pleistocene extensional tectonics in the Campidano graben (SW Sardinia, Italy): preliminary note. Rend. Online Soc. Geol. It. 29, 31–34.
Como, S., Magni, P., Baroli, M., Casu, D., De Falco, G., Floris, A., 2008. Comparative analysis of macrofaunal species richness and composition in Posidonia oceanica, Cymodocea nodosa and leaf litter beds. Mar. Biol. 153, 1087–1101. https://doi.org/10.1007/s00227-007-0881-z.
Conforti, A., Budillon, F., Tonielli, R., De Falco, G., 2016. A newly discovered Pliocene volcanic field on the western Sardinia continental margin (western Mediterranean). Geo-Mar. Lett. 36, 1–14.
Cooper, J.A.G., 1993. Sedimentation in a river dominated estuary. Sedimentology 40, 979–1017. https://doi.org/10.1111/j.1365-3091.1993.tb01372.x.
Cooper, J.A.G., Green, A.N., Wright, C.I., 2012. Evolution of an incised valley coastal plain estuary under low sediment supply: a 'give-up' estuary. Sedimentology 59, 899–916.
Crockett, J.S., Nittrouer, C.A., Ogston, A.S., Naar, D.F., Donahue, B.T., 2008. Morphology and filling of incised submarine valleys on the continental shelf near the mouth of the Fly River, Gulf of Papua. J. Geophys. Res. 113 https://doi.org/10.1029/2006JF000674.
Cucco, A., Perilli, A., De Falco, G., Ghezzo, M., Umgiesser, G., 2006. Water circulation and transport timescales in the Gulf of Oristano. Chem. Ecol. 22 (Suppl. 1), 307–331.
De Falco, G., Ferrari, S., Cancemi, G., Baroli, M., 2000. Relationships between sediment distribution and Posidonia oceanica seagrass. Geo-Mar. Lett. 20, 50–57.
De Falco, G., Baroli, M., Murru, E., Piergallini, G., Cancemi, G., 2006. Sediment analysis evidences two different depositional phenomena influencing seagrass distribution in the Gulf of Oristano (Sardinia—western Mediterranean). J. Coast. Res. 22 (5), 1043–1050.
De Falco, G., Baroli, M., Cucco, A., Simeone, S., 2008. Intrabasinal condition the development of a biogenic carbonate sedimentary facies associated seagrass Posidonia oceanica. Cont. Shelf Res. 28, 797–812.
De Falco, G., Tonielli, R., Di Martino, G., Innangi, S., Simeone, S., Parnum, I.M., 2010. Relationships between multibeam backscatter, sediment grain size, and Posidonia oceanica seagrass distribution. Cont. Shelf Res. 30, 1941–1950.
De Falco, G., Antonioli, F., Fontolan, G., Lo Presti, V., Simeone, S., Tonielli, 2015a. Early cementation and accommodation space dictate the evolution of barrier system during the Holocene. Mar. Geol. 369, 52–66.
De Falco, G., Budillon, F., Conforti, A., Di Bitetto, A., Di Martino, G., Innangi, S., Simeone, S., Tonielli, R., 2015b. Sorted bedforms over transgressive deposits along the continental shelf of western Sardinia (Mediterranean Sea). Mar. Geol. 359, 75–88.
De Falco, G., Molinaroli, E., Conforti, A., Simeone, S., Tonielli, R., 2017. Biogenic sediments from coastal ecosystems to beach–dune systems: implications for the adaptation of mixed and carbonate beaches to future sea level rise. Biogeosciences 14, 3191–3205.
Di Rita, F., Simone, O., Caldara, M., Gehrels, W.R., Magri, D., 2011. Holocene environmental changes in the coastal Tavoliere plain (Apulia, southern Italy): a multiproxy approach. Palaeogeogr. Palaeoclimatol. Palaeoecol. 310, 139–151.
Dladla, N.N., Green, A.N., Cooper, J.A.G., Humphriesc, M.S., 2019. Geological inheritance and its role in the geomorphological and sedimentological evolution of bedrock-hosted incised valleys, lake St Lucia, South Africa. Estuar. Coast. Shelf Sci. 222, 154–167.
Dladla, N.N., Green, A.N., Humphriesc, M.S., Cooper, J.A.G., Godfrey, M., Wright, C.I., 2022. Back-barrier evolution and along-strike variations in infilling of the Kosi Bay lake system, South Africa. Estuar. Coast. Shelf Sci. 272, 107877.
Engelbrecht, L., Green, A.N., Cooper, J.A.G., Hahn, A., Zabel, M., Mackay, C.F., 2020. Construction and evolution of submerged deltaic bodies on the high energy SE African coastline: the interplay between relative sea level and antecedent Controls. Mar. Geol. 424, 106170.
Flood, R.D., Hiscott, R.N., Aksu, A.E., 2009. Morphology and evolution of an anastomosed channel network where saline underflow enters the Black Sea. Sedimentology 56, 807–839.
Francolini, L., Lecca, L., Mazzei, R., 1990. La presenza del Pliocene inferiore nella piattaforma della Sardegna occidentale. Atti Soc. Tosc. Sci. Nat. Mem. Ser. A 97, 93–111.
Gensous, B., Tesson, M., 1996. Sequence stratigraphy, seismic profiles, and cores of Pleistocene deposits on the Rhône continental shelf. Mar. Geol. 105, 183–190.
Gomes, M.P., Vital, H., Stattegger, K., Schwarzer, K., 2016. Bedrock control on the Assu Incised Valley morphology and sedimentation in the Brazilian Equatorial Shelf Moab Praxedes. Int. J. Sediment Res. 31, 181–193.
Green, A.N., 2009. Palaeo-drainage, incised valley fills and transgressive systems tract sedimentation of the northern KwaZulu-Natal continental shelf, South Africa, SW Indian Ocean. Mar. Geol. 263, 46–63.
Green, A.N., Dladla, N.N., Garlick, L., 2013. The evolution of incised valley systems from the Durban continental shelf, KwaZulu-Natal, South Africa. Mar. Geol. 335, 148–161. https://doi.org/10.1016/j.margeo.2012.11.002.
Green, A.N., Cooper, J.A.G., Wiles, E.A., De Lecea, A.M., 2015. Seismic architecture, stratigraphy and evolution of a subtropical marine embayment: Maphuto Bay. Mozambique. Mar. Geol. 369, 300–309.
Green, A.N., Humphries, M.S., Cooper, J.A.G., Strachan, K.L., Gomes, M., Dladla, N.N., 2022. The Holocene evolution of Lake St Lucia, Africa's largest estuary: geological implications for contemporary management. Estuar. Coast. Shelf Sci. 266, 107745.
Greene Jr., D.L., Rodriguez, A.B., Anderson, J.B., 2007. Seaward-branching coastal-plain ad piedmont incised-valley systems through multiple sea-level cycles: Late Quaternary examples from Mobile bay and Mississippi Sound, U.S.A. J. Sediment. Res. 77, 139–158.
Gupta, S., Collier, J.S., Palmer-Felgate, A., Potter, G., 2007. Catastrophic flooding origin of shelf valley systems in the English Channel. Nature 448, 342–345.
Labaune, C., Tesson, M., Gensous, B., Parize, O., Imbert, P., Delhaye-Prat, V., 2010. Detailed architecture of a compound incised valley system and correlation with forced regressive wedges: example of Late Quaternary Têt and Agly rivers, western Gulf of Lions, Mediterranean Sea, France. Sediment. Geol. 223, 360–379.
Lambeck, K., Antonioli, F., Anzidei, M., Ferranti, L., Leoni, G., Scicchitano, G., Silenzi, S., 2011. Sea level change along the Italian coast during the Holocene and projections for the future. Quat. Int. 232, 250–257.
Langston, A.L., Temme, A.J.A.M., 2019. Impacts of lithologically controlled mechanisms on downstream bedrock valley widening. Geophys. Res. Lett. 46 https://doi.org/10.1029/2019GL085164.
Lericolais, G., Auffret, J.P., Bourillet, J.F., 2003. The Quaternary Channel River: seismic stratigraphy of its palaeo-valleys and deeps. J. Quat. Sci. 18, 245–260.
Liu, J.P., Milliman, J.D., Gao, S., Cheng, P., 2004. Holocene development of the yellow River's subaqueous delta, north yellow sea. Mar. Geol. 209, 45–67. https://doi.org/10.1016/j.margeo.2004.06.009.
Lobo, F.J., García, M., Luján, M., Mendes, I., Reguera, M.I., Van Rooij, D., 2017. Morphology of the last subaerial unconformity on a shelf: insights into transgressive ravinement and incised valley occurrence in the Gulf of Cádiz. Geo-Mar. Lett. https://doi.org/10.1007/s00367-017-0511-9.
Mancini, M., Tilocca, G., 2007. Relazione monografica di bacino idrografico, fiume TirsoProgetto di piano stralcio delle fasce fluviali. Technical Report available on. https://www.regione.sardegna.it/.
Martin, J., Cantelli, A., Paola, C., Blum, M., Wolinsky, M., 2011. Quantitative modeling of the evolution and geometry of incised valley. J. Sediment. Res. 81, 64–79.
Maselli, V., Trincardi, F., 2013. Large-scale single incised valley from a small catchment basin on the western Adriatic margin (central Mediterranean Sea). Glob. Planet. Chang. 100, 245–262.
Maselli, V., Trincardi, F., Asioli, A., Ceregato, A., Rizzetto, F., Taviani, M., 2014. Delta growth and river valleys: the influence of climate and sea level changes on the South Adriatic shelf (Mediterranean Sea). Quat. Sci. Rev. 99, 146–163.
Matthews, C.R., Rodriguez, A.B., 2011. Controls on late Quaternary incised-valley dimension along passive margins evaluated using empirical data. Sedimentology 58, 1113–1137.
Mccave, I.N., Hall, I.R., 2006. Size sorting in marine muds: processes, pitfalls, and prosects for paleoflow-speed proxies. Geochem. Geophys. Geosyst. 7. Q10N05.
Melis, R.T., Depalmas, A., Di Rita, F., Montisa, F., Vacchi, M., 2017. Mid to late Holocene environmental changes along the coast of western Sardinia (Mediterranean Sea). Glob. Planet. Chang. 155, 29–41.
Mellett, C.L., Hodgson, D.M., Mauz, B., Lang, A., Selby, I., Plater, A.J., 2012. Preservation of a drowned gravel barrier complex: a landscape evolution study from the northeastern English Channel. Mar. Geol. 315–318, 115–131.
Mitchum, J.R., Vail, P.R., Sangree, J.B., 1977. Stratigraphic interpretation of seismic reflection pattern in depositional sequences. In: Payton, C.E. (Ed.), Seismic Stratigraphy—Applications to Hydrocarbon Exploration, AAPG Memoirs, 26, pp. 117–134.
Pascucci, V., De Falco, G., Del Vais, C., Sanna, I., Melis, R.T., Andreucci, S., 2018. Climate changes and human impact on the Mistras coastal barrier system (W Sardinia, Italy). Mar. Geol. 395, 271–284.

Perry, C.A., Hsu, K.J., 2000. Geophysical, archaeological, and historical evidence support a solar-output model for climate change. Proc. Natl. Acad. Sci. 97, 12433–12438.
Posamentier, H.W., 2001. Lowstand alluvial bypass systems: incised vs. unincised. AAPG Bull. 85 (10), 1771–1793 (October 2001).
Pretorius, L., Green, A., Cooper, J., Hahn, A., Zabel, M., 2019. Outer- to inner-shelf response to stepped sea-level rise: insights from incised valleys and submerged shorelines. Mar. Geol. 416, 105979.
Qiu, J., Liu, J., Saito, Y., Yin, P., Zhang, Y., Liu, J., Zhou, L., 2019. Seismic morphology and infilling architecture of incised valleys in the northwest South Yellow Sea since the last glaciations. Cont. Shelf Res. 179, 52–65.
Rydin, H., Jeglum, J.K., 2013. The Biology of Peatlands, 2 eds. Oxford University Press, Oxford UK. 432 pp.
Salzmann, L., Green, A., Cooper, J.A.G., 2013. Submerged barrier shoreline sequences on a high energy, steep and narrow shelf. Mar. Geol. 346, 366–374.
Sarti, G., Rossi, V., Amorosi, A., Bini, M., Giacomelli, S., Pappalardo, M., Ribecai, C., Ribolini, A., Sammartino, I., 2015. Climatic signature of two mid–late Holocene fluvial incisions formed under sea-level highstand conditions (Pisa coastal plain, NW Tuscany, Italy). Palaeogeogr. Palaeoclimatol. Palaeoecol. 424, 183–195.
Schumm, S.A., 1993. River response to base level change: implications for sequence stratigraphy. J. Geol. 101, 279–294.
Shan, X., Yu, X., Clift, P.D., Tan, C., LI, S., Wang, Z., SU, D., 2016. Ground-penetrating radar study of beach-ridge deposits in Huangqihai Lake, North China: the imprint of washover processes. Front. Earth Sci. 10 (1), 183–194. https://doi.org/10.1007/s11707-015-0501-z.
Simeone, S., De Falco, G., Quattrocchi, G., Cucco, A., 2014. Morphological changes of a Mediterranean beach over oneyear (San Giovanni di Sinis, western Mediterranean). J. Coast. Res. 70, 217–222.
Simms, A.R., Aryal, N., Miller, L., Yokoyama, Y., 2010. The incised valley of Baffin Bay, Texas: a tale of two climates. Sedimentology 57, 642–669.
Stuiver, M., Reimer, P.J., Reimer, R.W., 2022. CALIB 8.2 (WWW program) at. http://calib.org.
Tanabe, S., Hori, K., Saito, Y., Haruyama, S., Vu, V.P., Kitamura, A., 2003. Song Hong (Red River) delta evolution related to millennium-scale Holocene sea-level change. Quat. Sci. Rev. 22, 2345–2361. https://doi.org/10.1016/S0277-3791(03)00138-0.
Tanabe, S., Nakanishi, T., Ishihara, Y., Nakashima, R., 2015. Millennial-scale stratigraphy of a tide-dominated incised valley during the last 14 kyr: spatial and quantitative reconstruction in the Tokyo Lowland, central Japan. Sedimentology 62, 1837–1872. https://doi.org/10.1111/sed.12204.
Tesson, M., Labaune, C., Gensous, B., Suc, J.-P., Melinte-Dobrinescu, M., Parize, O., Imbert, P., Delhaye-Prat, V., 2011. Quaternary "compound" incised valley in a microtidal environment, Roussillon Continental shelf, western Gulf of Lions, France. J. Sediment. Res. 81, 708–729.
Thieler, E.R., Butman, B., Schwab, W.C., Allison, M.A., Driscoll, N.W., Donnelly, J.P., Uchupi, E., 2007. A catastrophic meltwater flood event and the formation of Hudson Shelf Valley. Palaeogeogr. Palaeoclimatol. Palaeoecol. 246, 120–136.
Thomas, M.A., Anderson, J.B., 1994. Sea-level controls on the facies architecture of the Trinity/Sabine incised-valley system, Texas continental shelf. In: Dalrymple, R.W., Boyd, R., Zaitlin, B.A. (Eds.), Incised-valley System: Origin and Sedimentary Sequences. SEPM Special Publication, vol. 51. SEPM, Society for Sedimentary Geology, Tulsa, Oklahoma, USA, pp. 63–83.
Traini, C., Menier, D., Proust, J.-N., Sorrel, P., 2013. Transgressive systems tract of a ria-type estuary: The Late Holocene Vilaine River drowned valley (France). Mar. Geol. 337, 140–155.
Vacchi, M., Marriner, N., Morhange, C., Spada, G., Fontana, A., Rovere, A., 2016. Multiproxy assessment of Holocene relative sea-level changes in the western Mediterranean: sea-level variability and improvements in the definition of the isostatic signal. Earth-Sci. Rev. 155, 172–197. https://doi.org/10.1016/j.earscirev.2016.02.002.
Vacchi, M., Ghilardi, M., Melis, R.T., Spada, G., Giaime, M., Marriner, N., Lorscheid, T., Morhange, C., Burjachs, F., Rovere, A., 2018. New relative sea-level insights into the isostatic history of the Western Mediterranean. Quat. Sci. Rev. 201, 396–408.
Vacchi, M., Joyse, K.M., Kopp, R.E., Marriner, N., Kaniewski, D., Rovere, A., 2021. Climate pacing of millennial sea-level change variability in the central and western Mediterranean. Nat. Commun. 12, 4013. https://doi.org/10.1038/s41467-021-24250-1.
Walsh, K., 2014. The Archaeology of Mediterranean Landscapes: Human-Environment Interaction. Cambridge University Press (365 pp.).
Wang, R., Colombera, L., Mountney, N.P., 2019. Geological controls on the geometry of incised-valley fills: Insights from a global dataset of late-Quaternary examples. Sedimentology 66, 2134–2168.
Wang, R., Colombera, L., Mountney, N.P., 2020. Quantitative analysis of the stratigraphic architecture of incised-valley fills: a global comparison of Quaternary systems. Earth Sci. Rev. 200, 102988.
Ximenes Neto, A.R., Silva Pessoa, P.R., de Souza Pinheiro, L., Onofre de Morais, J., 2022. Seismic stratigraphy of a partially filled incised valley on a semi-arid continental shelf, Northeast Brazil. Geo-Mar. Lett. 41, 18.
Zaitlin, B.A., Dalrymple, R.W., Boyd, R., 1994. The stratigraphic organization of incised-valley systems associated with relative sea-level change. In: Dalrymple, R.W., Boyd, R., Zaitlin, B.A. (Eds.), Incised-valley System: Origin and Sedimentary Sequences. SEPM Special Publication, vol. 51. SEPM, Society for Sedimentary Geology, Tulsa, Oklahoma, USA, pp. 45–60.
Zanchetta, G., Drysdale, R.N., Hellstrom, J.C., Fallick, A.E., Isola, I., Gagan, M., Pareschi, M.T., 2007. Enhanced rainfall in the western Mediterranean during deposition of sapropel S1: stalagmite evidence from Corchia cave (Central Italy). Quat. Sci. Rev. 26, 279–286.
Zanchetta, G., Regattieri, E., Isola, I., Drysdale, R.N., Bini, M., Baneschi, I., Hellstrom, J., 2016. The so-called "4.2 event" in the Central Mediterranean and its climatic teleconnections. Alpine Mediterran. Quatern. 29 (1), 5–17.
Zhornyak, L.V., Zanchetta, G., Drysdale, R.N., Hellstrom, J.C., Isola, I., Regattieri, E., Piccini, L., Baneschi, I., Couchoud, I., 2011. Stratigraphic evidence for a "pluvial phase" between ca 8200–7100 ka from Renella Cave (Central Italy). Quat. Sci. Rev. 30, 409–417.